Title: Ultrafast high-endurance memory based on sliding ferroelectrics

Authors: Kenji Yasuda[1,2†*], Evan Zalys-Geller[1†], Xirui Wang[1], Daniel Bennett[3], Suraj S Cheema[4], Kenji Watanabe[5], Takashi Taniguchi[6], Efthimios Kaxiras[3,7], Pablo Jarillo-Herrero[1*], and Raymond Ashoori[1*]

[1]Department of Physics, Massachusetts Institute of Technology, Cambridge, Massachusetts, USA.

[2]School of Applied and Engineering Physics, Cornell University, Ithaca, New York 14850, USA.

[3]John A. Paulson School of Engineering and Applied Sciences, Harvard University, Cambridge, Massachusetts 02138, USA

[4]Research Laboratory of Electronics, Massachusetts Institute of Technology, Cambridge, Massachusetts, USA.

[5]Research Center for Electronic and Optical Materials, National Institute for Materials Science, Tsukuba 305-0044, Japan

[6]Research Center for Materials Nanoarchitectonics, National Institute for Materials Science, Tsukuba 305-0044, Japan

[7]Department of Physics, Harvard University, Cambridge, Massachusetts 02138, USA.

[†]These authors contributed equally to this work

[*]Correspondence to: kenji.yasuda@cornell.edu, pjarillo@mit.edu, ashoori@mit.edu

Abstract: The persistence of voltage-switchable collective electronic phenomena down to the atomic scale has extensive implications for area-efficient and energy-efficient electronics, especially in emerging nonvolatile memory technology. We investigate the performance of a ferroelectric field-effect transistor (FeFET) based on sliding ferroelectricity in bilayer boron nitride at room temperature. Sliding ferroelectricity represents a different form of atomically thin two-dimensional ferroelectrics, characterized by the switching of out-of-plane polarization through interlayer sliding motion. We examined the FeFET device employing monolayer graphene as the channel layer, which demonstrated ultrafast switching speeds on the nanosecond scale and high endurance exceeding 10^{11} switching cycles, comparable to state-of-the-art FeFET devices. These characteristics highlight the potential of two-dimensional sliding ferroelectrics for inspiring next-generation nonvolatile memory technology.

Main Text:

The quest for a high-speed nonvolatile memory that is voltage-driven and high-endurance for low-power and reliable operation remains a long-standing challenge towards addressing the explosion of data in modern technology. A promising candidate technology for energy-efficient nonvolatile memory is the ferroelectric field-effect transistor (FeFET), where the electrical conductance and threshold voltage of the channel layer is controlled by switching the electric polarization of an adjacent ferroelectric layer by an applied electric field. Despite intensive efforts to integrate conventional ferroelectrics into nonvolatile memory technology, challenges remain such as endurance and thickness scaling, underscoring the need for novel ferroelectric materials. Discovery of certain ferroelectric materials, such as fluorite-structure HfO_2-ZrO_2 (*1*) and wurtzite-structure AlN-ScN (*2*), has triggered a resurgence of interest in FeFET memory. These three-dimensional (3D) materials stand out due to their robust ferroelectric properties even in the ultra-thin limit (*3*, *4*), which opens avenues for the development of energy-efficient and scalable FeFETs (*5*). Another emerging category of ultrathin ferroelectrics is two-dimensional (2D) van der Waals materials. The absence of dangling bonds and conventional ferroelectric size effects in these materials enables ferroelectricity down to a thickness of a few layers (*6*, *7*), offering promising pathways for next-generation device applications.

2D materials, due to their stacking degrees of freedom, also offer a different pathway to ferroelectricity in comparison to their 3D ferroelectric counterparts, which can potentially improve nonvolatile memory operation. Recently, a type of 2D ferroelectricity, known as sliding ferroelectrics, was discovered, where the polarization is switched through the interlayer sliding motion (*8*). This sliding motion is enabled by the weak van der Waals nature of the interlayer bonding of layered 2D materials. Sliding ferroelectricity appears in exfoliated 2D materials from bulk crystals such as WTe_2 and $MoTe_2$ (*9*, *10*), as well as in artificially stacked van der Waals heterostructures of 2D materials. For example, boron nitride (BN) (*11–13*) and semiconducting transition metal dichalcogenides (TMDs), such as MoS_2 (*14–16*), can be made ferroelectric by altering the stacking orders from their natural configurations. This synthetic approach to ferroelectricity has expanded the category of 2D ferroelectrics to a much broader range of 2D materials with exceptional physical properties.

We show a schematic illustration of commonly used bulk hexagonal BN (hBN) crystals (Fig. 1A). Each layer consists of a honeycomb lattice made of boron and nitrogen atoms, stacked in an AA’ configuration, meaning one layer of BN is rotated 180 degrees with respect to the other. Because of this 180-degree rotated stacking order, bulk hBN is centrosymmetric and non-ferroelectric. Meanwhile, using the van der Waals assembly technique established for 2D materials, artificially creating a new stacking order is possible where two layers of BN are stacked in parallel, a 0-degree orientation. In this configuration, BN adopts either an AB or BA stacking order (Fig. 1B) which are energetically degenerate. As the space group is rhombohedral in these stacking orders, parallel-stacked BN is also called rhombohedral BN. Because of the vertical alignment of boron and nitrogen atoms, interlayer charge transfer occurs from the nitrogen atom to the boron atom, creating a finite electric dipole moment and macroscopic electrical polarization. For the AB stacking configurations, the boron atom is located above the nitrogen atom, while in the BA stacking configuration, the nitrogen atom is located above the boron atom. Accordingly, these two different stacking orders lead to out-of-plane electrical polarization in the upward and downward directions, respectively, as can be seen from mirror symmetry breaking of differential charge distribution. Previous experimental work demonstrated

that these AB and BA stackings transform between each other by applying a vertical electric field (*11*, *12*). The switching occurs through the interlayer sliding motion, namely, by shifting one layer by 1/3 of the unit cell. The unconventional coupling between in-plane sliding motion and out-of-plane polarization switching is unique to these materials, and this ferroelectricity is referred to as sliding ferroelectricity.

Parallel-stacked bilayer BN, consisting of two atomic sheets, exhibits robust sliding ferroelectricity at room temperature, despite its miniscule thickness of 0.67 nm. This property positions it as a promising candidate for the development of energy-efficient nanoscale FeFETs, as the required voltage for the switching scales with the material's thickness. Notably, BN serves as an exceptional environmental protection layer for other 2D materials, such as graphene and TMDs, leading to higher mobility and an enhanced on/off ratio. Consequently, investigating the ferroelectric characteristics of BN is of critical importance in advancing next-generation device applications based on 2D materials and van der Waals heterostructures (*17*). We constructed a van der Waals heterostructure-based FeFET, utilizing monolayer graphene as the channel layer, to evaluate the switching speed and endurance of ferroelectric BN. We discovered that it exhibits nanosecond scale ferroelectric switching speed, and a high endurance of 10^{11} switching cycles, comparable to the best values reported in HfO_2-based FeFETs (*18–20*).

Basic characterization

For our device structure, we sandwiched a monolayer graphene between top and bottom bulk hBN (Fig. 1C). These hBN layers possess conventional AA' stacking and are non-ferroelectric, which we use as gate dielectrics. We inserted parallel-stacked bilayer BN layer that exhibits sliding ferroelectricity. Depending on the out-of-plane polarization direction of the parallel-stacked bilayer BN, either negative or positive charge is injected into the graphene monolayer. This allows us to determine the ferroelectric polarization direction by measuring the graphene's resistance. We conducted all measurements under vacuum at room temperature.

Considering the graphene's resistance as a function of the gate voltage V_G (Fig. 1D), we observed a peak in resistance, corresponding to the charge neutrality condition of graphene. Unlike conventional graphene FET devices, however, we observe hysteresis as a function of gate voltage. The green and brown curves are forward and backward scans, respectively. We found a prominent hysteresis depending on the scanning direction of the gate voltage. As we applied the voltage between graphene and the gate, the electric field is applied to the parallel-stacked bilayer BN, which results in the switching of the out-of-plane polarization. Furthermore, the resistance exhibited abrupt changes around $V_G = 1.85$ V and $V_G = -0.9$ V, which stems from the ferroelectric polarization switching from down-to-up and up-to-down, respectively.

Ultrafast switching of sliding ferroelectrics

We explored the pulse width dependence of the switching voltage. We first initialized the polarization to the up state by applying $V_G = 2.5$ V. We then applied a voltage pulse with varying lengths and widths. After this, we measured the resistance of the graphene sensing layer at $V_G = 0.21$ V to check if polarization had switched (Fig. 2A, upper portion). $V_G = 0.21$ V is the charge neutrality condition of the up-polarization state. Therefore, the red (blue) color in the color plot indicates up (down) polarization. We also performed a similar procedure by initializing the polarization to down by applying $V_G = -2.5$ V and applying a pulse with varying lengths and widths (Fig. 2B). We investigated switching kinetics over 10 orders of magnitude in time, from 1 ns to 10 s for up to down polarization switching and from 1 ns to 5 s for down to up polarization

switching. The critical voltage for polarization switching increases as the pulse width decreases (Fig. 2), in accordance with classic models of ferroelectric switching kinetics (*21–23*). Crucially, we can switch the device's polarization switching with a pulse width as short as 1 ns for both up-to-down and down-to-up polarization switching. The switching speed of 1 ns is only limited by our instrumentation and by the design of the device, which is not optimized for RF signals. Despite these limitations, our device's measured performance is comparable to that of state-of-the-art HfO_2-based FeFET devices (*24*).

The ferroelectric switching occurs through ferroelectric domain wall motion. The coercive field expected for coherent homogeneous switching is 7.8 V/nm (*8*, *25*). Meanwhile, the experimentally obtained coercive field is 0.3 V/nm, more than twenty times smaller than the estimated value for coherent switching. This discrepancy tells us that the switching occurs via the domain nucleation and growth rather than the uniform switching of the entire device. This observation is consistent with the real space imaging of electric-field induced domain wall motion of sliding ferroelectrics based on scanning probe (*12*, *14*, *26*) and electron microscopy techniques (*15*, *16*). Assuming that the switching happens through the motion of a single domain wall, we calculate the domain wall speed to be as high as 1000 m/s, by dividing the device size of around 1 μm by the pulse width of 1 ns. This ultrafast domain wall speed is consistent with theoretical predictions (*27*), and is much faster than the previously reported speed of 300 μm/s in sliding ferroelectric WSe_2 (*16*). The shorter pulse we applied enabled the observation of the ultrafast domain wall motion in our system, which could be useful for domain wall-based nanoelectronics (*28*).

The domain wall speed is approaching the speed of shear phonon modes of around 18000 m/s (*29*), which should be the physical limitation of the domain wall motion. Investigating how domain wall dynamics change when driven close to phonon speeds would be interesting as it might involve relativistic motion, as demonstrated for ferromagnetic domain wall motion (*30*). Real-space imaging will be invaluable for understanding the dynamics of ferroelectric switching in sliding ferroelectricity from both fundamental and application perspectives (*11*, *12*, *14–16*, *26*, *31*). Going further, coherent and uniform switching of the entire layer may even be possible with ultrafast optical light on a picosecond-timescale (*32–34*).

High endurance of sliding ferroelectrics

We measured the endurance of ferroelectric switching. We started by applying single pulses with a width of 100 ns and a height of V_{pulse} = 3.1 V and V_{pulse} = −3.1 V repeatedly up to 1.11×10^4 switching cycles. Next, we applied a square wave with a peak height of ±3.1 V with up to frequency of 10^7 Hz for variable durations of time. After the application of the square wave, we applied two voltage pulses of V_{pulse} = 3.1 V and V_{pulse} = −3.1 V each with the width of 100 ns and measured the graphene's resistance at V_G = 0.15 V to confirm that the ferroelectric property was not degraded (Fig. 3). V_G = 0.15 V is the charge neutrality condition of the up-polarization state, which drifted slightly from that in Fig. 2. The switching properties of ferroelectric BN remain almost unchanged over 10^{11} switching cycles (Fig. 3), as seen from the polarization switching by the voltage pulses. We further verified that the magnitude of polarization and the coercive field remains almost unchanged after the switching cycle (fig. S2).

The fatigueless switching we observed in our FeFET devices, exceeding 10^{11} cycles without altering the ferroelectric characteristics, is comparable to the best performing FeFET devices reported in HfO_2 (*18–20*). The high endurance in ferroelectric BN was achieved without any

optimization of the sample or device structure. The high endurance in HfO_2, required over ten years of optimization of the interfacial layers (*1*, *5*, *18–20*). The superior endurance of our devices underscores the inherent robustness of polarization switching in sliding ferroelectrics. The degradation of conventional FeFETs over extensive switching typically originates from the creation of defects at the interfacial layer between the ferroelectrics and the channel layer. These defects lead to premature breakdown in the interfacial layer and a decrease in polarization and memory window in the ferroelectric layer (*35*). Unlike conventional switching mechanisms that involve switching ionic dipoles, sliding ferroelectrics rely on the in-plane sliding motion between the layers bonded by physical van der Waals force. We speculate that these characteristics prevent the creation of defects at the interface or that any defects created in each layer do not affect the sliding motion, contributing to the high endurance of sliding ferroelectrics.

Conclusion

The combination of ultrafast switching and high endurance, together with subnanometer thickness, sub-3.3-V operation required for embedded memory, and retention exceeding one month (*11*), underscore the potential of sliding ferroelectrics in nonvolatile memory technology (see table S1). At the same time, there are several critical challenges that remain to be addressed for practical applications. One major challenge is achieving wafer-scale synthesis of sliding ferroelectrics, which could be realized by advancing existing growth techniques of rhombohedral BN, such as chemical vapor deposition and sputtering (*36–40*). Another challenge is improving the on/off ratio. The inherently small polarization in sliding ferroelectrics results in limited on/off ratio in the FeFET geometry. This challenge can be addressed by adopting a device geometry that relies not on the absolute magnitude of polarization but rather on the band alignment between the layers. For example, a sliding ferroelectric MoS_2 device has recently achieved on/off ratios that span six orders of magnitude in a ferroelectric semiconductor field-effect transistor geometry that utilizes the ferroelectric semiconductor itself as the channel layer (*41*). Although technological integration challenges remain, 2D-based FeFET memory technology is currently being pursued by semiconductor foundries (*42*). We anticipate that our research demonstrating superior nonvolatile memory performance derived from a novel mechanism of ferroelectric switching will spur further research into nonvolatile memory technology based on sliding ferroelectrics.

References and Notes

1. T. S. Böscke, J. Müller, D. Bräuhaus, U. Schröder, U. Böttger, Ferroelectricity in hafnium oxide thin films. *Appl Phys Lett* **99**, 102903 (2011).
2. K. H. Kim, I. Karpov, R. H. Olsson, D. Jariwala, Wurtzite and fluorite ferroelectric materials for electronic memory. *Nat Nanotechnol* **18**, 422–441 (2023).
3. H.-J. Lee, M. Lee, K. Lee, J. Jo, H. Yang, Y. Kim, S. Chul Chae, U. Waghmare, J. H. Lee, Scale-free ferroelectricity induced by flat phonon bands in HfO2. *Science (1979)* **369**, 1343–1347 (2020).
4. S. S. Cheema, N. Shanker, S.-L. Hsu, Y. Rho, C.-H. Hsu, V. A. Stoica, Z. Zhang, J. W. Freeland, P. Shafer, C. P. Grigoropoulos, J. Ciston, S. Salahuddin, Emergent ferroelectricity in subnanometer binary oxide films on silicon. *Science (1979)* **376**, 648–652 (2022).
5. U. Schroeder, M. H. Park, T. Mikolajick, C. S. Hwang, The fundamentals and applications of ferroelectric HfO2. *Nat Rev Mater* **7**, 653–669 (2022).
6. M. Wu, J. Li, Sliding ferroelectricity in 2D van der Waals materials: Related physics and future opportunities. *Proc Natl Acad Sci U S A* **118**, 50 (2021).
7. D. Zhang, P. Schoenherr, P. Sharma, J. Seidel, Ferroelectric order in van der Waals layered materials. *Nat Rev Mater* **8**, 25–40 (2023).
8. L. Li, M. Wu, Binary Compound Bilayer and Multilayer with Vertical Polarizations: Two-Dimensional Ferroelectrics, Multiferroics, and Nanogenerators. *ACS Nano* **11**, 6382–6388 (2017).
9. Z. Fei, W. Zhao, T. A. Palomaki, B. Sun, M. K. Miller, Z. Zhao, J. Yan, X. Xu, D. H. Cobden, Ferroelectric switching of a two-dimensional metal. *Nature* **560**, 336–339 (2018).
10. A. Jindal, A. Saha, Z. Li, T. Taniguchi, K. Watanabe, J. C. Hone, T. Birol, R. M. Fernandes, C. R. Dean, A. N. Pasupathy, D. A. Rhodes, Coupled ferroelectricity and superconductivity in bilayer Td-MoTe2. *Nature* **613**, 48–52 (2023).
11. K. Yasuda, X. Wang, K. Watanabe, T. Taniguchi, P. Jarillo-Herrero, Stacking-engineered ferroelectricity in bilayer boron nitride. *Science (1979)* **372**, 1458–1462 (2021).
12. M. Vizner Stern, Y. Waschitz, W. Cao, I. Nevo, K. Watanabe, T. Taniguchi, E. Sela, M. Urbakh, O. Hod, M. Ben Shalom, Interfacial ferroelectricity by van der Waals sliding. *Science (1979)* **372**, 1462–1466 (2021).
13. C. R. Woods, P. Ares, H. Nevison-Andrews, M. J. Holwill, R. Fabregas, F. Guinea, A. K. Geim, K. S. Novoselov, N. R. Walet, L. Fumagalli, Charge-polarized interfacial superlattices in marginally twisted hexagonal boron nitride. *Nat Commun* **12**, 347 (2021).
14. X. Wang, K. Yasuda, Y. Zhang, S. Liu, K. Watanabe, T. Taniguchi, J. Hone, L. Fu, P. Jarillo-Herrero, Interfacial ferroelectricity in rhombohedral-stacked bilayer transition metal dichalcogenides. *Nat Nanotechnol* **17**, 367–371 (2022).
15. A. Weston, E. G. Castanon, V. Enaldiev, F. Ferreira, S. Bhattacharjee, S. Xu, H. Corte-León, Z. Wu, N. Clark, A. Summerfield, T. Hashimoto, Y. Gao, W. Wang, M. Hamer, H. Read, L. Fumagalli, A. V. Kretinin, S. J. Haigh, O. Kazakova, A. K. Geim, V. I. Fal'ko, R. Gorbachev, Interfacial ferroelectricity in marginally twisted 2D semiconductors. *Nat Nanotechnol* **17**, 390–395 (2022).
16. K. Ko, A. Yuk, R. Engelke, S. Carr, J. Kim, D. Park, H. Heo, H. M. Kim, S. G. Kim, H. Kim, T. Taniguchi, K. Watanabe, H. Park, E. Kaxiras, S. M. Yang, P. Kim, H. Yoo, Operando electron microscopy investigation of polar domain dynamics in twisted van der Waals homobilayers. *Nat Mater* **22**, 992–998 (2023).

17. C. Liu, H. Chen, S. Wang, Q. Liu, Y. G. Jiang, D. W. Zhang, M. Liu, P. Zhou, Two-dimensional materials for next-generation computing technologies. *Nat Nanotechnol* **15**, 545–557 (2020).
18. S. De, D. D. Lu, H.-H. Le, S. Mazumder, Y.-J. Lee, W.-C. Tseng, B.-H. Qiu, M. Aftab Baig, P.-J. Sung, C.-J. Su, C.-T. Wu, W.-F. Wu, W.-K. Yeh, Y.-H. Wang, "Ultra-Low Power Robust 3bit/cell Hf0.5Zr0.5O2 Ferroelectric FinFET with High Endurance for Advanced Computing-In-Memory Technology" in *2021 Symposium on VLSI Technology* (IEEE, 2021)vol. 1, pp. 1–2.
19. A. J. Tan, Y. H. Liao, L. C. Wang, N. Shanker, J. H. Bae, C. Hu, S. Salahuddin, Ferroelectric HfO2Memory Transistors with High-κ Interfacial Layer and Write Endurance Exceeding 1010Cycles. *IEEE Electron Device Letters* **42**, 994–997 (2021).
20. M. C. Nguyen, S. Kim, K. Lee, J. Y. Yim, R. Choi, D. Kwon, Wakeup-free and Endurance-robust Ferroelectric Field-Effect Transistor Memory Using High Pressure Annealing. *IEEE Electron Device Letters* **42**, 1295–1298 (2021).
21. Y. Ishibashi, Y. Takagi, Note on Ferroelectric Domain Switching. *J Physical Soc Japan* **31**, 506–510 (1971).
22. M. Avrami, Kinetics of phase change. I: General theory. *J Chem Phys* **7**, 1103–1112 (1939).
23. A. K. Tagantsev, I. Stolichnov, N. Setter, J. S. Cross, M. Tsukada, Non-Kolmogorov-Avrami switching kinetics in ferroelectric thin films. *Phys Rev B Condens Matter Mater Phys* **66**, 214109 (2002).
24. M. M. Dahan, H. Mulaosmanovic, O. Levit, S. Dünkel, S. Beyer, E. Yalon, Sub-Nanosecond Switching of Si:HfO2 Ferroelectric Field-Effect Transistor. *Nano Lett* **23**, 1395–1400 (2023).
25. Materials and methods are available as Supplementary Materials on Science Online.
26. M. Lv, X. Sun, Y. Chen, T. Taniguchi, K. Watanabe, M. Wu, J. Wang, J. Xue, Spatially Resolved Polarization Manipulation of Ferroelectricity in Twisted hBN. *Advanced Materials* **34**, 2203990 (2022).
27. R. He, B. Zhang, H. Wang, L. Li, P. Tang, G. Bauer, Z. Zhong, Ultrafast switching dynamics of the ferroelectric order in stacking-engineered ferroelectrics. *Acta Mater* **262**, 119416 (2024).
28. D. Meier, S. M. Selbach, Ferroelectric domain walls for nanotechnology. *Nat Rev Mater* **7**, 157–173 (2022).
29. R. J. Jiménez-Riobóo, L. Artús, R. Cuscó, T. Taniguchi, G. Cassabois, B. Gil, In- and out-of-plane longitudinal acoustic-wave velocities and elastic moduli in h -BN from Brillouin scattering measurements. *Appl Phys Lett* **112**, 051905 (2018).
30. L. Caretta, S.-H. Oh, T. Fakhrul, D.-K. Lee, B. H. Lee, K. Kim, C. A. Ross, K.-J. Lee, G. S. D. Beach, Relativistic kinematics of a magnetic soliton. *Science (1979)* **370**, 1438–1442 (2020).
31. C. R. Woods, P. Ares, H. Nevison-Andrews, M. J. Holwill, R. Fabregas, F. Guinea, A. K. Geim, K. S. Novoselov, N. R. Walet, L. Fumagalli, Charge-polarized interfacial superlattices in marginally twisted hexagonal boron nitride. *Nat Commun* **12**, 347 (2021).
32. J. Park, I. W. Yeu, G. Han, C. S. Hwang, J. H. Choi, Ferroelectric switching in bilayer 3R MoS2 via interlayer shear mode driven by nonlinear phononics. *Sci Rep* **9**, 14919 (2019).
33. H. Xu, J. Zhou, Y. Li, R. Jaramillo, J. Li, Optomechanical control of stacking patterns of h-BN bilayer. *Nano Res* **12**, 2634–2639 (2019).

34. R. Mankowsky, A. Von Hoegen, M. Först, A. Cavalleri, Ultrafast Reversal of the Ferroelectric Polarization. *Phys Rev Lett* **118**, 197601 (2017).
35. E. Yurchuk, S. Mueller, D. Martin, S. Slesazeck, U. Schroeder, T. Mikolajick, J. Müller, J. Paul, R. Hoffmann, J. Sundqvist, T. Schlösser, R. Boschke, R. van Bentum, M. Trentzsch, "Origin of the Endurance Degradation in the Novel HfO2-based 1T Ferroelectric Non-Volatile Memories" in *2014 IEEE International Reliability Physics Symposium* (IEEE, 2014).
36. M. Chubarov, H. Pedersen, H. Högberg, J. Jensen, A. Henry, Growth of high quality epitaxial rhombohedral boron nitride. *Cryst Growth Des* **12**, 3215–3220 (2012).
37. P. Sutter, J. Lahiri, P. Zahl, B. Wang, E. Sutter, Scalable synthesis of uniform few-layer hexagonal boron nitride dielectric films. *Nano Lett* **13**, 276–281 (2013).
38. S. M. Gilbert, T. Pham, M. Dogan, S. Oh, B. Shevitski, G. Schumm, S. Liu, P. Ercius, S. Aloni, M. L. Cohen, A. Zettl, Alternative stacking sequences in hexagonal boron nitride. *2d Mater* **6**, 021006 (2019).
39. L. Souqui, J. Palisaitis, N. Ghafoor, H. Pedersen, H. Högberg, Rhombohedral boron nitride epitaxy on ZrB2. *Journal of Vacuum Science & Technology A: Vacuum, Surfaces, and Films* **39**, 013405 (2021).
40. L. Wang, J. Qi, W. Wei, M. Wu, Z. Zhang, X. Li, H. Sun, Q. Guo, M. Cao, Q. Wang, C. Zhao, Y. Sheng, Z. Liu, C. Liu, M. Wu, Z. Xu, W. Wang, H. Hong, P. Gao, M. Wu, Z. J. Wang, X. Xu, E. Wang, F. Ding, X. Zheng, K. Liu, X. Bai, Bevel-edge epitaxy of ferroelectric rhombohedral boron nitride single crystal. *Nature* **629**, 74–79 (2024).
41. T. H. Yang, B. W. Liang, H. C. Hu, F. X. Chen, S. Z. Ho, W. H. Chang, L. Yang, H. C. Lo, T. H. Kuo, J. H. Chen, P. Y. Lin, K. B. Simbulan, Z. F. Luo, A. C. Chang, Y. H. Kuo, Y. S. Ku, Y. C. Chen, Y. J. Huang, Y. C. Chang, Y. F. Chiang, T. H. Lu, M. H. Lee, K. S. Li, M. Wu, Y. C. Chen, C. L. Lin, Y. W. Lan, Ferroelectric transistors based on shear-transformation-mediated rhombohedral-stacked molybdenum disulfide. *Nat Electron* **7**, 29–38 (2023).
42. T.-E. Lee, H.-L. Chiang, C.-Y. Chang, Y.-C. Su, S.-J. Chang, J.-J. Wu, B.-J. Lin, J.-F. Wang, S.-C. Haw, S.-J. Chiu, H.-L. Ching, Y.-G. Lin, W.-S. Yun, C.-F. Hsu, H. Lee, T.-Y. Lee, M. Passlack, C.-C. Cheng, C.-S. Chang, H.-S. P. Wong, W.-H. Chang, M.-F. Chang, Y.-M. Lin, I. P. Radu, "High-Endurance MoS 2 FeFET with Operating Voltage Fess Than IV for eNVM in Scaled CMOS Technologies" in *2023 International Electron Devices Meeting (IEDM)* (IEEE, 2024).
43. DOI: 10.5061/dryad.1jwstqk3c
44. K. Momma, F. Izumi, VESTA 3 for three-dimensional visualization of crystal, volumetric and morphology data. *J Appl Crystallogr* **44**, 1272–1276 (2011).
45. J. M. Soler, E. Artacho, J. D. Gale, A. García, J. Junquera, P. Ordejón, D. Sánchez-Portal, The SIESTA method for ab initio order-N materials simulation. *J. Phys.: Condens. Matter* **14**, 2745–2779 (2002).
46. M. J. van Setten, M. Giantomassi, E. Bousquet, M. J. Verstraete, D. R. Hamann, X. Gonze, G. M. Rignanese, The PSEUDODOJO: Training and grading a 85 element optimized norm-conserving pseudopotential table. *Comput Phys Commun* **226**, 39–54 (2018).
47. M. Dion, H. Rydberg, E. Schröder, D. C. Langreth, B. I. Lundqvist, Van der Waals density functional for general geometries. *Phys Rev Lett* **92**, 246401 (2004).

48. V. R. Cooper, Van der Waals density functional: An appropriate exchange functional. *Phys Rev B Condens Matter Mater Phys* **81**, 161104 (2010).
49. M. J. Rutter, C2x: A tool for visualisation and input preparation for Castep and other electronic structure codes. *Comput Phys Commun* **225**, 174–179 (2018).
50. S. P. Beckman, X. Wang, K. M. Rabe, D. Vanderbilt, Ideal barriers to polarization reversal and domain-wall motion in strained ferroelectric thin films. *Phys Rev B Condens Matter Mater Phys* **79**, 144124 (2009).
51. L. Tong, Z. Peng, R. Lin, Z. Li, Y. Wang, X. Huang, K.-H. Xue, H. Xu, F. Liu, H. Xia, P. Wang, M. Xu, W. Xiong, W. Hu, J. Xu, X. Zhang, L. Ye, X. Miao, 2D materials-based homogeneous transistor-memory architecture for neuromorphic hardware. *Science (1979)* **373**, 1353–1358 (2021).
52. K. H. Kim, S. Oh, M. M. A. Fiagbenu, J. Zheng, P. Musavigharavi, P. Kumar, N. Trainor, A. Aljarb, Y. Wan, H. M. Kim, K. Katti, S. Song, G. Kim, Z. Tang, J. H. Fu, M. Hakami, V. Tung, J. M. Redwing, E. A. Stach, R. H. Olsson, D. Jariwala, Scalable CMOS back-end-of-line-compatible AlScN/two-dimensional channel ferroelectric field-effect transistors. *Nat Nanotechnol* **18**, 1044–1050 (2023).
53. X. Wang, C. Zhu, Y. Deng, R. Duan, J. Chen, Q. Zeng, J. Zhou, Q. Fu, L. You, S. Liu, J. H. Edgar, P. Yu, Z. Liu, Van der Waals engineering of ferroelectric heterostructures for long-retention memory. *Nat Commun* **12**, 1109 (2021).
54. M. Si, A. K. Saha, S. Gao, G. Qiu, J. Qin, Y. Duan, J. Jian, C. Niu, H. Wang, W. Wu, S. K. Gupta, P. D. Ye, A ferroelectric semiconductor field-effect transistor. *Nat Electron* **2**, 580–586 (2019).
55. S. Wang, L. Liu, L. Gan, H. Chen, X. Hou, Y. Ding, S. Ma, D. W. Zhang, P. Zhou, Two-dimensional ferroelectric channel transistors integrating ultra-fast memory and neural computing. *Nat Commun* **12**, 3665 (2021).
56. W. Han, X. Zheng, K. Yang, C. S. Tsang, F. Zheng, L. W. Wong, K. H. Lai, T. Yang, Q. Wei, M. Li, W. F. Io, F. Guo, Y. Cai, N. Wang, J. Hao, S. P. Lau, C. S. Lee, T. H. Ly, M. Yang, J. Zhao, Phase-controllable large-area two-dimensional In2Se3 and ferroelectric heterophase junction. *Nat Nanotechnol* **18**, 55–63 (2023).

Acknowledgments: We thank Tomas Palacios for fruitful discussions. This work was primarily supported by the by the Army Research Office MURI W911NF2120147, the 2DMAGIC MURI FA9550-19-1-0390, the MIT/Microsystems Technology Laboratories Samsung Semiconductor Research Fund, the National Science Foundation (DMR-1809802), the Gordon and Betty Moore Foundation's EPiQS Initiative through grant GBMF9463, and the Ramon Areces Foundation. Work from EZG and RA was supported by U.S. Department of Energy, Office of Science, Basic Energy Sciences, under Award Number DE-SC0020149. KW and TT acknowledge support from the JSPS KAKENHI (Grant Numbers 21H05233 and 23H02052) and World Premier International Research Center Initiative (WPI), MEXT, Japan**.** This work was performed in part at the Harvard University Center for Nanoscale Systems (CNS); a member of the National Nanotechnology Coordinated Infrastructure Network (NNCI), which is supported by the National Science Foundation under NSF award no. ECCS-2025158. This work was carried out in part through the use of MIT.nano's facilities. This work made use of the MRSEC Shared Experimental Facilities at MIT, supported by the National Science Foundation under award number DMR-1419807.

Funding:

Army Research Office MURI W911NF2120147 (EK, PJH)

2DMAGIC MURI FA9550-19-1-0390 (PJH)

MIT/Microsystems Technology Laboratories Samsung Semiconductor Research Fund (PJH)

National Science Foundation DMR-1809802 (PJH)

Gordon and Betty Moore Foundation's EPiQS Initiative GBMF9463 (PJH)

Ramon Areces Foundation (PJH)

Department of Energy, Office of Science, Basic Energy Sciences, DE-SC0020149 (RA)

World Premier International Research Center Initiative (WPI), MEXT (KW, TT)

JSPS KAKENHI grants 21H05233 and 23H02052 (KW, TT)

Author contributions:

Conceptualization: KY, EZG

Investigation: KY, EZG, XW

Resources: KW, TT

Formal analysis: DB, SSC, EK

Supervision: PJH, RA

Writing – original draft: KY

Writing – review & editing: KY, SSC, EZG, XW, DB, PJH, RA

Competing interests: Authors declare that they have no competing interests.

Data and materials availability: The data shown in the paper is available from (*43*).

Supplementary Materials

Materials and Methods

Supplementary Text

Figs. S1 to S5

Table. S1

References (*45*–*56*)

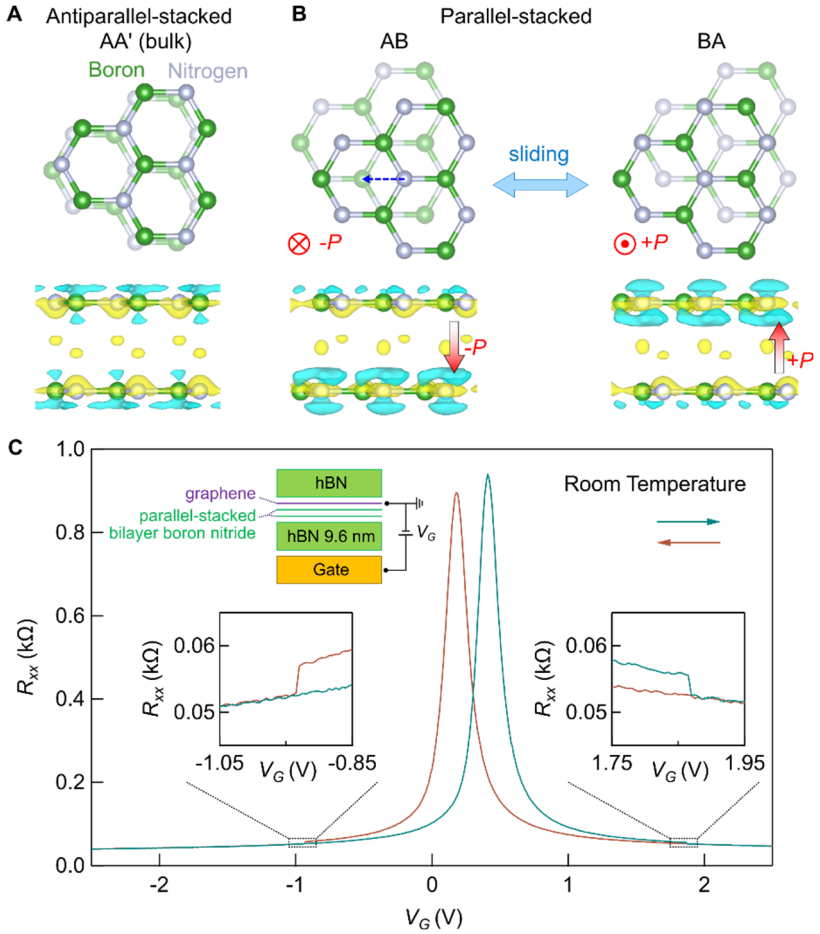

Fig. 1. Basic characteristics of a ferroelectric field-effect transistor based on sliding ferroelectrics. (A) Schematic of the crystal structure of antiparallel-stacked bilayer boron nitride with AA' stacking. Nitrogen and boron atoms are displayed in silver and green, respectively. The bottom panel shows the differential charge distribution mapping. The yellow and blue region corresponds to the increased negative and positive charge as compared to a monolayer, respectively. The figures are drawn using VESTA (*44*). **(B)** Schematic of the crystal structures of parallel-stacked bilayer boron nitride. AB and BA stacking creates out-of-plane ferroelectric polarization in opposite directions, which can be switched by the interlayer sliding motion which is denoted by the dotted blue line. **(C)** Resistance of monolayer graphene R_{xx} as a function of the gate voltage V_G. The green and brown curves correspond to forward and backward scans, respectively. The inset shows the schematic of the side view of the ferroelectric field-effect transistor, and enlarged view at the ferroelectric switching voltages.

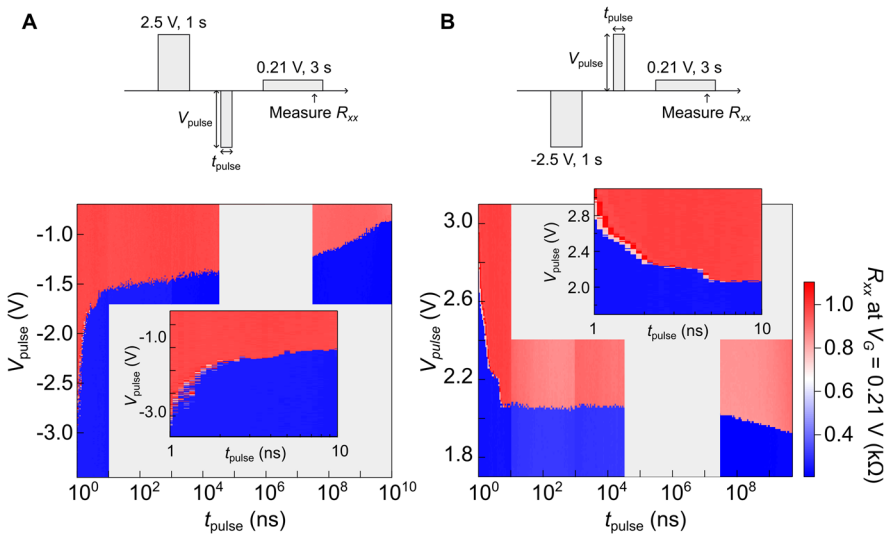

Fig. 2. Pulse width dependence of switching voltage. (**A**) Top: Illustration of the measurement procedure. Bottom: Resistance of monolayer graphene R_{xx} measured at V_G = 0.21 V after the application of negative voltage pulse of V_{pulse} and t_{pulse}. The inset shows the enlarged view from 1 ns to 10 ns. We could not apply well-defined pulse between 30 ms and 30 μs due to significant distortion of the pulse shape because of the bias tee placed near the sample (fig. S1). This region is shaded in gray. (**B**) The same as **A** for the positive voltage pulses.

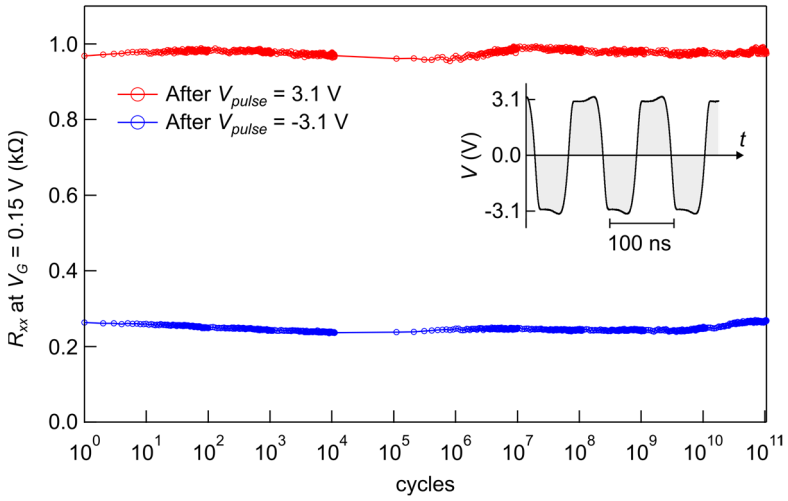

Fig. 3. Endurance of sliding ferroelectrics against switching cycles. Resistance of monolayer graphene R_{xx} measured at $V_G = 0.15$ V after the sets of voltage pulse or ac square voltage, followed by the application of voltage pulses of $V_{pulse} = -3.1$ V and $V_{pulse} = 3.1$ V with pulse width of 100 ns. The inset shows the shape of the ac square voltage with 10^7 Hz measured by an oscilloscope.